Turkish Journal of Physics

http://journals.tubitak.gov.tr/physics/

Review Article

Turk J Phys
(2020) 44: 239 – 246

doi:10.3906/fiz-2004-20

On-chip quantum optics and integrated optomechanics

David HOCH[1,2,3], **Timo SOMMER**[1,2], **Sebastian MÜLLER**[1], **Menno POOT**[1,2,3,*]
[1]Department of Physics, Technical University Munich, Garching, Germany
[2]Munich Center for Quantum Science and Technology (MCQST), Munich, Germany
[3]Institute for Advanced Study, Technical University Munich, Garching, Germany

Received: 20.04.2020 • **Accepted/Published Online:** 02.06.2020 • **Final Version:** 22.06.2020

Abstract: Recent developments in quantum computing and the growing interest in optomechanics and quantum optics need platforms that enable rapid prototyping and scalability. This can be fulfilled by on-chip integration, as we present here. The different nanofabrication steps are explained, and our automated measurement setup is discussed. We present an opto-electromechanical device, the H-resonator, which enables optomechanical experiments such as electrostatic springs and nonlinearities and thermomechanical squeezing. Moreover, it also functions as an optomechanical phase shifter, an essential element for our integrated quantum optics efforts. Besides this, the equivalent of a beam splitter in photonics-the directional coupler-is shown. Its coupling ratio can be reliably controlled, as we show with experimental data. Several directional couplers combined can realize the CNOT operation with almost ideal fidelity.

Key words: Integrated quantum optics, optomechanics, squeezing, feedback

1. Introduction

Quantum science is rapidly making the step towards quantum technology. One of its goals is to develop quantum computers that outperform classical ones [1, 2]. One of many approaches is to use photons as qubits and linear optical components as operations [3, 4]. This approach is often referred to as linear optical quantum computing (LOQC)[4, 5] . A major challenge is that all optical components need to be aligned, which becomes more and more complex with an increasing size of the experiments. Our approach [6, 7] is to use integrated photonic circuits. Here, many components can be realized on a single chip without the need of aligning every individual one. Scaling thus becomes a matter of nanofabrication. Besides integrated quantum optics, we apply the same approach to optomechanics. First, it is discussed how the photonic chips are fabricated and measured. In the second part, this is illustrated with the opto-electromechanical "H-resonator" [8]. Thirdly, we focus on the photonic circuitry for the integrated quantum optics experiments, in particular on directional couplers and CNOT operations. As an outlook, we discuss the integration of sources and detectors on the same chip. This shows that our approach provides a promising platform for quantum experiments.

2. Device fabrication and setup

Typically, we study large sets of optical components on a chip with varying parameters, e.g. optomechanical devices or building blocks for LOQC. Figure 1(a) shows a small subset of the 108 devices on that chip. Calibration devices, as shown e.g., in the top 3 rows, are also included. For reproducibly measuring many

*Correspondence: menno.poot@tum.de

devices, the highly automated setup in Figure 1(b) is used. There, the polarization of light from a fiber-coupled sweep laser is adjusted by a fiber polarization controller. An x-y stage positions the chip underneath an array of fibers. One of these illuminates a grating coupler, which are used to couple light into and out of the devices (Figure 1(a), inset) [9]. Other fibers lead to photodetectors. An automated routine locates the devices and optimizes the position for maximal optical transmission.

A histogram for 100 different optimizations of the transmitted power is shown in Figure 1(c). The small ($< 0.3\%$) spread indicates the reproducibility of the measurement process. For the devices, high-stress silicon nitride (SiN) is used, which combines low losses in the infrared with excellent mechanical properties [6, 10]. Figure 2(a) shows the starting point of the nanofabrication. The SiO_2 serves as a cladding layer for the waveguides. In the first step (Figure 2(b)) gold markers and electrodes are made by evaporation and lift-off. The markers are essential for the alignment of further lithography steps. In the second step (Figure 2(c)), patterns are etched into the SiN by reactive ion etching. Depending on the etch depth, (i) waveguides are formed, or (ii) mechanical structures are prepared. The latter are released using buffered hydrofluoric acid (BHF), resulting in the final structure in Figure 2(d).

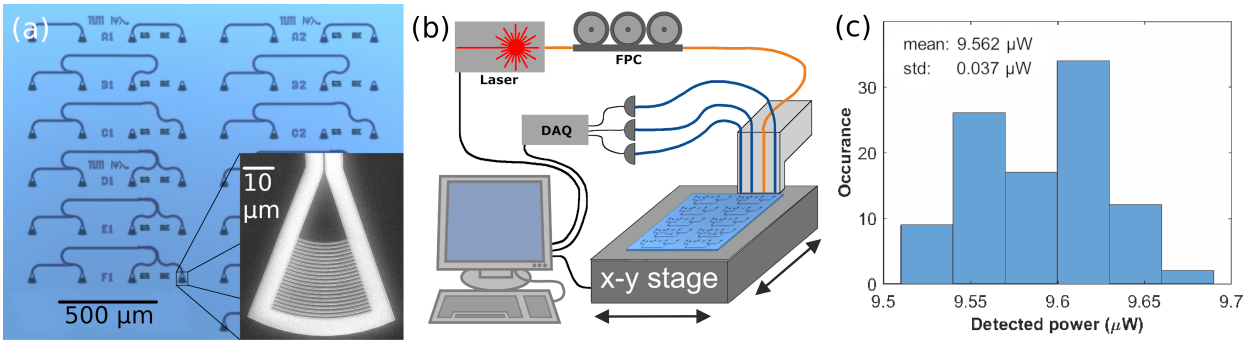

Figure 1. (a) Micrograph of a chip with directional coupler devices. The inset shows a scanning electron micrograph (SEM) of a grating coupler. (b) Schematic of the measurement setup with a sweep laser (1480 to 1640 nm), fiber polarization controller (FPC), motorized x-y stage, and data-acquisition system (DAQ) to measure the photodetectors. (c) Histogram of the detected power for 100 optimizations of the chip position underneath the fiber array.

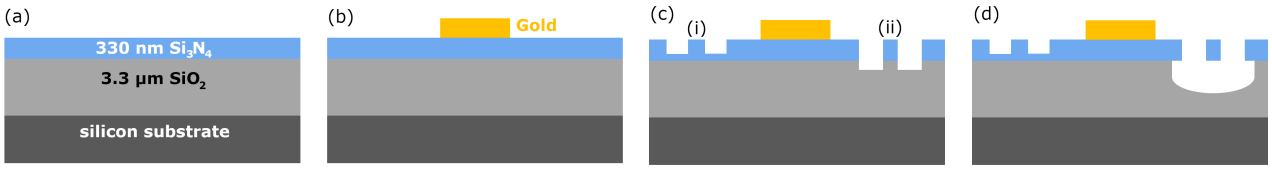

Figure 2. Nanofabrication steps for optomechanical devices. (a) Starting wafer. (b) Deposition of metallic markers and electrodes. (c) Reactive ion etching of SiN in 2 separate steps: (i) Patterning of the photonic circuits with $\sim$ 20 nm SiN remaining. (ii) Definition of the mechanical structures by etching all the way into the silicon oxide. (d) The latter are released by immersing the entire chip in BHF, followed by critical point drying.

3. Phase shifter and optomechanics

Optomechanics is a rapidly developing field where mechanical resonators are studied using the most sensitive detection method: light [11–13]. Optomechanical resonators can range from km-long gravitational wave de-

tectors to nanometer-sized devices [14]. Our H-resonator is another example. Its broad application ranges from optical phase shifting in LOQC (Section. 4) [8] to optomechanics experiments. The resonator shown in Figure 3(a,b) consists of a central block tethered by 4 arms, forming an H-shape. A voltage is applied between a fixed electrode and one on the H displaces the structure in plane, changing the distance to an adjacent waveguide d_{opt}. The photons in the waveguide see this change in the dielectric environment. This changes the effective refractive index n_{eff} (Figure 3(c)) and thus the phase $\phi = 2\pi n_{\mathrm{eff}} L/\lambda_0$ that a photon acquires after propagating a distance L. Here $\lambda_0 \sim 1550\,\mathrm{nm}$ is the free-space wavelength. Figure 3(d) shows the measured optical phase shift vs. the applied voltage V. Its parabolic shape originates from the electrostatic force, which is $\propto V^2$. Importantly, the block of the H-resonator contains a photonic crystal to prevent photons leaking from the waveguide. Furthermore, the electrodes are placed far away from the waveguide to minimize absorption.

A big advantage of the H-resonator over other phase shifters, e.g., the widely-used thermo-optic devices, is its much lower dissipation. This enables operation at the cryogenic temperatures required for superconducting detectors. Our optomechanical phase shifter operates for a large wavelength range, only limited by the bandwidth of the waveguide, and works from single photons to much higher powers; only at Watts of optical power, gradient forces would influence the mechanical phase shifting [8]. For the first generation of devices, phase shifts larger than 90° were obtained [8]. This can be improved by e.g., changing the actuation from pulling to pushing, or by cascading multiple devices.

Besides static operation, one can also study the dynamic performance of the H-resonator. Figure 3(e) shows its measured frequency response; the device can be operated up to a few MHz. The peaks are the mechanical modes shown in the insets. In air, their quality factor Q lies around 10. For phase shifting a flatter response may be desirable, but for optomechanics reduced dissipation is wanted. This can be done by placing the chip in vacuum. Below $10^{-2}\,\mathrm{mBar}$, Qs up to $200,000$ are possible, as shown in Figure 3(f), enabling state-of-the-art optomechanics experiments.

Next, we discuss the electrostatic interactions in the H-resonator. These are large enough to strongly tune its resonance frequency as shown in Figure 4(a). The resonance frequency is shifted by more than 25 % by making use of the so-called electrostatic spring effect [15]. Besides the electrostatic tuning of its frequency, also the nonlinear response of the resonator can be controlled electrically. Purely mechanical systems typically become stiffer when driven to large amplitudes. In contrast, the driven responses in Figure 4(b) show a bending of the resonance to the left with increasing driving powers. In this case, the nonlinearity of the device is no longer mechanical, but electrostatic in nature.

Optomechanics is capable of resolving much smaller displacements than the amplitudes of 10s of nm in Figure 4(b). With a typical sensitivity of 20 $\mathrm{fm/Hz^{1/2}}$, the thermal motion ($\sim 18\,\mathrm{pm}$) of our devices can not only be resolved with a good signal-to-noise ratio, but also manipulated; squeezing is a powerful technique where the uncertainty in one quadrature is reduced at the expense of the other. This is typically done by pumping the resonator at twice its resonance frequency [16]. First, we will discuss how the thermal motion of the H-resonator was squeezed and how feedback is essential for this, followed by a short discussion on how this could be extended to true quantum squeezing. The thermal motion was measured via an on-chip Mach-Zehnder interferometer and demodulated using a lockin amplifier. From this, the probability density function (PDF) of its motion in phase space and the variances (width of the PDF) are determined [17]. As illustrated in Figure 5(a), the variances of the X- and Y-quadrature change; they are proportional to $\gamma/(\gamma \pm \chi)$, respectively, where γ is the original damping rate and χ is proportional to V_P, the 2f parametric pump amplitude. Thus, as the ellipsoidal

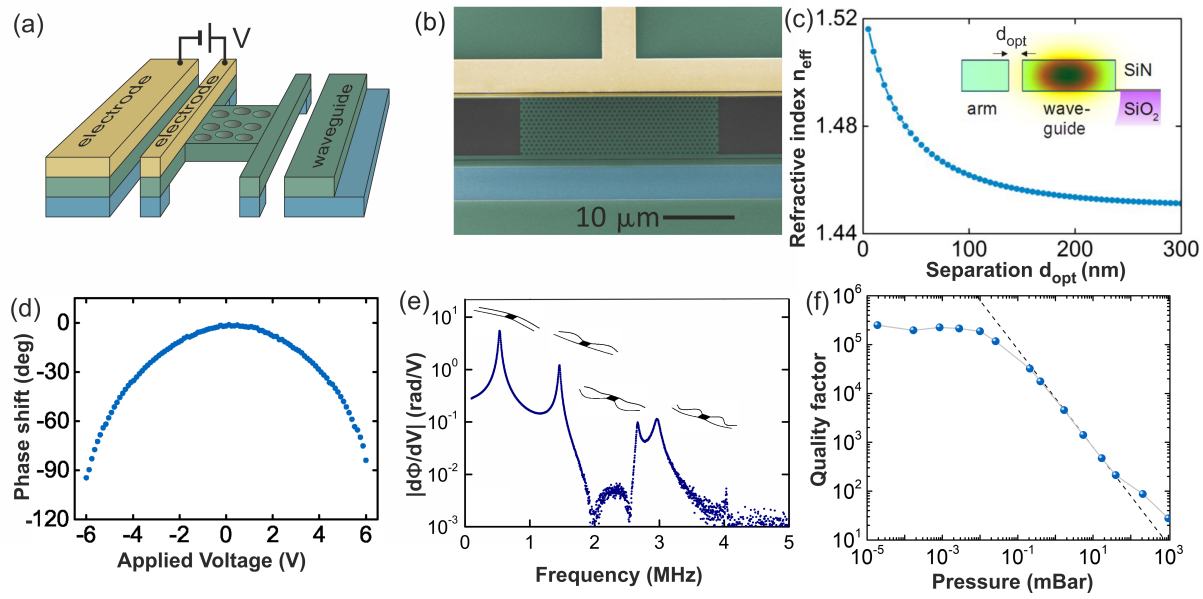

Figure 3. (a) Sketch of an H-resonator. A voltage between the electrodes actuates the resonator, changing its distance to the waveguide. (b) Colorized SEM of the central part of an H-resonator. (c) Dependence of n_{eff} on d_{opt} simulated using a finite-elements method. The inset shows the optical mode. (d) Phase shift vs. the voltage. (e) Frequency response of the phase shifter. The peaks correspond to its eigenmodes (insets, calculated using finite-elements). (f) Pressure dependence of the Q of the fundamental in-plane flexural mode. The dashed line shows the linear dependence of Q in the transition from high to low pressures.

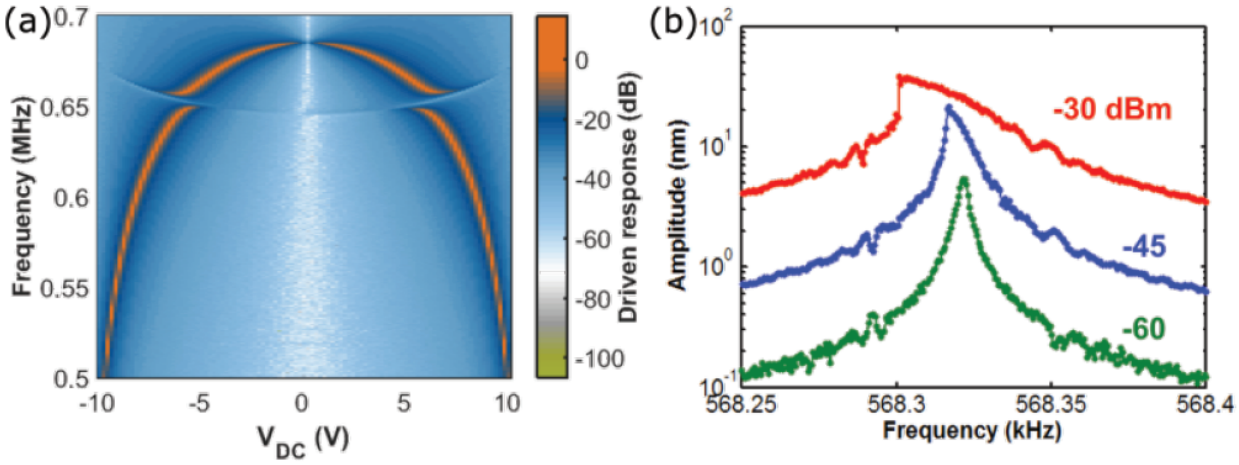

Figure 4. (a) Driven response of an H-resonator vs. the applied voltage. Strong tuning of the resonance frequency due to the electrostatic spring effect is visible. (b) Response for different driving powers, showing electrostatic weakening.

PDF in the inset shows, 2f pumping leads to squeezing in X and amplification in Y. When χ becomes equal to γ, the damping in Y vanishes, resulting a divergence of the fluctuations. This sets the so-called 3 dB limit for parametric squeezing [16].

A way to overcome this is to stabilize the Y quadrature with feedback [17, 18]. Without feedback gain ($g = 0$) the squeezing is limited to 3 dB (Figure 5(b)), but when feeding the measured Y signal back

with $g = 10$, V_P can be increased further. However, the achieved squeezing does not exceed the reduction in Y without pumping. Still, this combined technique does not underlie any fundamental limit and 15 dB was achieved at $g = 100$ [17]. So far, these measurements were done at room temperature. By applying this technique to GHz resonators cooled down to mK temperatures, the *quantum* zero-point motion can be squeezed, leading to true squeezed states. It is also possible to do nonlinear (the feedback on Y is linear) feedback via the phase. This can be used to generate non-Gaussian states [19]. These are few examples of the possibilities of integrated optomechanics.

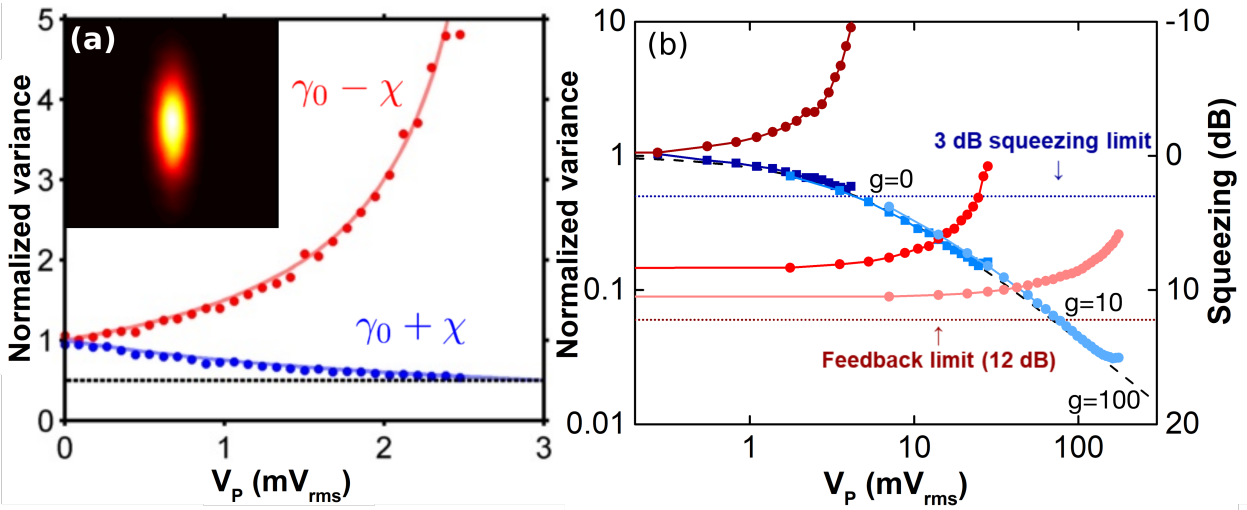

Figure 5. (a) Normalized variance of the X- and Y-quadratures over the pump power V_P. The inset shows the squeezed PDFs at $V_P = 2.47\,\mathrm{mV_{rms}}$. (b) Parametric pumping combined with feedback. When using the pump only (X: dark blue; Y: brown), the squeezing of the X-quadrature is limited by the 3 dB squeezing limit. When pumping and Y-feedback are combined (X: blue; Y: red) X is squeezed further. At a gain of 100 V/V (X: light blue; Y: light red) 15 dB of squeezing was achieved, widely surpassing both the squeezing and feedback cooling limits.

4. Linear optical quantum computing

A second topic where the power of photonic circuits is becoming more and more apparent, is integrated quantum optics. In this case, the experiments that used to be done on huge optical tables filled with carefully aligned optical components are now performed on chips. This enables the development of large-scale quantum optics circuits, such as needed for e.g., quantum computing. Quantum computing requires qubits to store quantum information, and a set of single- and multi-qubit operations [1]. In our approach-integrated LOQC - the qubit is naturally represented by a single photon in 1 of 2 separate waveguides. In this so-called dual-rail encoding [1, 4] operations are implemented in photonic circuits. One often-used single-qubit operation is the phase shift. By combining it with beam splitters, also the important 2-qubit operation controlled-not (CNOT), where a control qubit determines the operation on a target qubit, can be realized [20]. Thus, *any* unitary quantum operation can be implemented with just 2 components [1, 4]. Phase shifting can naturally be performed by our H-resonator (Section 3), which also allows programming the quantum computer via the applied voltage. The equivalent of a beam splitter in photonics is the directional coupler (DC). There, 2 waveguides are brought close to one another so that their modes evanescently couple. The length of that interaction, L_{int} determines the amount of light that crosses over. A device to characterize this (Figure 6(a)) consists of 4 grating couplers

(GCs), waveguides, and the DC. Light enters via the second GC. With a Y-splitter [21] half of the light is split to the reference GC (left). The other half goes to the DC (top-right). Measuring the power at the 2 right GCs, which are connected to the outputs of the DC - in combination with calibration devices - gives the coupling ratio C, the normalized amount of light that crosses over to the other waveguide. Figure 6(b) shows the measured C of devices with different L_{int}, as shown in Figure 6(b). The fit [22] allows finding L_{int} for a desired coupling ratio [6]. As shown in Figure 6(d), the CNOT operation requires $C = 1/2$ and $2/3$. These values are indicated in Figure 6(b). Intersections with the fit (arrows) yield the required L_{int} for the desired coupling ratios for $\lambda_0 = 1550\,\text{nm}$. In Figure 6(c) their wavelength dependence is shown. Future work is to reduce this dispersion. A CNOT flips the target qubit depending on the state of the control qubit using DCs arranged as in Figure 6(d). It relies on interference between the different paths. In particular, if the control qubit is in the $|0\rangle_c$ state, it interferes with the target qubit at the 2/3 DC and prevents the flip of the target qubit. For $|1\rangle_c$ this does not happen and the combined effect of the two 1/2 DCs is a flip of the target qubit. However, the photons might end up in a wrong waveguide; these events must be excluded by postselection. This makes LOQC intrinsically probabilistic; the probability of success of this CNOT is 1/9 [20]. Still, when the experiment is postselected, it should, of course, give the correct outcome [23, 24]. The performance of our CNOT circuit is shown in Figure 6(e). Comparing it to an ideal CNOT (dotted) shows a good agreement, and a fidelity of 99.81% is extracted [6]. These measurements were still done with transmission measurements. However, for the quantum computing applications that we envision, much more complex photonic circuits will be used. These then will require more advanced characterization methods [7].

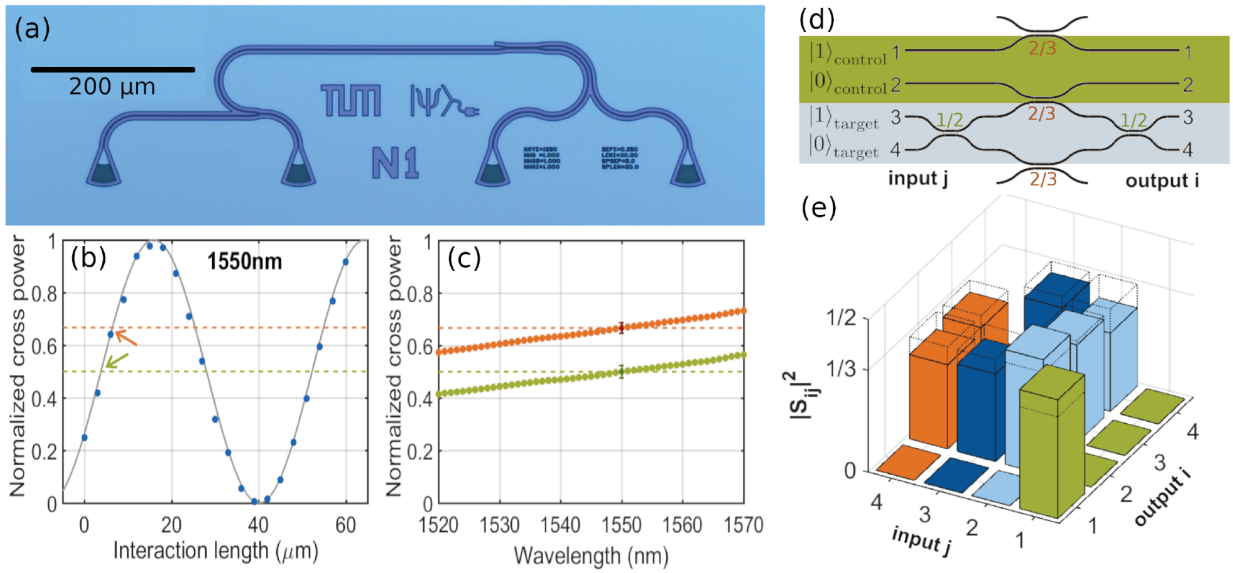

Figure 6. (a) Micrograph of a device to measure a single DC. (b) Measured coupling ratios vs. L_{int} and the $\sin^2$ fit (solid line). The dashed lines indicate $C = 1/2$ (green) and $2/3$ (orange), respectively. (c) Dispersion of C calculated using fits as in panel (b) for $L_{\text{int}} = 3.8$ (green) and $6.4\,\mu$m (orange). (d) Schematic of a CNOT circuit consisting of 5 DCs. The 2 waveguides highlighted in green represent the control qubit, whereas the ones in gray are the target qubit. With the parameters extracted from (b), a new chip with CNOT devices is made and measured. (e) The measured transmissions (bars) are very close to those for an ideal CNOT gate (dotted).

5. Outlook

To further improve the efficiency of our experiments, we are currently working on the integration of single-photon sources and detectors into the experiments on a single chip. The former can be done with spontaneous parametric down-conversion in AlN [25]. A promising alternative is the photo-luminescence from 2d materials [26]. Integrated superconducting nanowires will enable single-photon detection with almost unity quantum efficiency [27, 28]. These experiments will be performed at cryogenic temperatures, where also the optomechanical squeezing experiments will be continued.

Acknowledgment

This article is based on MP's talk at the Tübitak TBAE workshop on Quantum Frontiers of Technology (Gebze, Nov. 2019). The research is funded by the German Research Foundation (DFG) under Germany's Excellence Strategy - EXC-2111 - 390814868 and TUM-IAS, funded by the German Excellence Initiative and the European Union Seventh Framework Programme under grant agreement 291763.

References

[1] Nielsen MA, Chuang IL. Quantum computation and quantum information. Cambridge University Press, Cambridge, 2010.

[2] Arute F, Arya K, Babbush R, Bacon D, Bardin JC, Barends R, et al. Quantum supremacy using a programmable superconducting processor. Nature 2019; 574 (7779): 505–510. doi: 10.1038/s41586-019-1666-5

[3] Kok P, Munro WJ, Nemoto K, Ralph TC, Dowling JP, et al. Linear optical quantum computing with photonic qubits. Rev Mod Phys 2007; 79: 135–174. doi: 10.1103/RevModPhys.79.135

[4] Knill E, Laflamme R, Milburn GJ. A scheme for efficient quantum computation with linear optics. Nature 2001; 409 (6816): 46–52.

[5] O'Brien JL, Furusawa A, Vuckovic J. Photonic quantum technologies. Nature Photonics 2009; 3 (12): 687–695.

[6] Poot M, Schuck C, Ma Xs, Guo X, Tang HX. Design and characterization of integrated components for SiN photonic quantum circuits. Opt Express 2016; 24 (7): 6843–6860. doi: 10.1364/OE.24.006843

[7] Poot M, Tang HX. Characterization of optical quantum circuits using resonant phase shifts. Appl Phys Lett 2016; 109 (13): 131106. doi: 10.1063/1.4962902

[8] Poot M, Tang HX. Broadband nanoelectromechanical phase shifting of light on a chip. Appl Phys Lett 2014; 104 (6): 061101. doi: 10.1063/1.4864257

[9] Taillaert D, Bogaerts W, Bienstman P, Krauss T, Van Daele P, et al. An out-of-plane grating coupler for efficient butt-coupling between compact planar waveguides and single-mode fibers. Quantum Electronics, IEEE Journal of 2002; 38 (7): 949–955. doi: 10.1109/JQE.2002.1017613

[10] Fong KY, Pernice WHP, Li M, Tang HX. High Q optomechanical resonators in silicon nitride nanophotonic circuits. Appl Phys Lett 2010; 97 (7): 073112. doi: 10.1063/1.3480411

[11] Poot M, van der Zant HSJ. Mechanical systems in the quantum regime. Phys Rep 2012; 511 (5): 273–335. doi: 10.1016/j.physrep.2011.12.004

[12] Aspelmeyer M, Kippenberg TJ, Marquardt F. Cavity optomechanics. Rev Mod Phys 2014; 86: 1391–1452. doi: 10.1103/RevModPhys.86.1391

[13] Kippenberg TJ, Vahala KJ. Cavity optomechanics: back-action at the mesoscale. science 2008; 321 (5893): 1172–1176. doi: 10.1126/science.1156032

[14] Sun X, Zheng J, Poot M, Wong CW, Tang HX. Femtogram Doubly Clamped Nanomechanical Resonators Embedded in a High-Q Two-Dimensional Photonic Crystal Nanocavity. Nano Letters 2012; 12 (5): 2299–2305. doi: 10.1021/nl300142t

[15] Rieger J, Faust T, Seitner MJ, Kotthaus JP, Weig EM. Frequency and Q factor control of nanomechanical resonators. Appl Phys Lett 2012; 101 (10): 103110. doi: 10.1063/1.4751351

[16] Rugar D, Grütter P. Mechanical parametric amplification and thermomechanical noise squeezing. Phys Rev Lett 1991; 67 (6): 699–702. doi: 10.1103/PhysRevLett.67.699

[17] Poot M, Fong KY, Tang HX. Deep feedback-stabilized parametric squeezing in an opto-electromechanical system. New J Phys 2015; 17 (4): 043056. doi: 10.1088/1367-2630/17/4/043056

[18] Vinante A, Falferi P. Feedback-Enhanced Parametric Squeezing of Mechanical Motion. Phys Rev Lett 2013; 111: 207203. doi: 10.1103/PhysRevLett.111.207203

[19] Poot M, Fong KY, Tang HX. Classical non-Gaussian state preparation through squeezing in an optoelectromechanical resonator. Phys Rev A 2014; 90: 063809. doi: 10.1103/PhysRevA.90.063809

[20] Ralph TC, Langford NK, Bell TB, White AG. Linear optical controlled-NOT gate in the coincidence basis. PhysRev A 2002; 65: 062324. doi: 10.1103/PhysRevA.65.062324

[21] Zhang Y, Yang S, Lim AEJ, Lo GQ, Galland C, et al. A compact and low loss Y-junction for submicron silicon-waveguide. Opt Express 2013; 21 (1): 1310–1316. doi: 10.1364/OE.21.001310

[22] Huang WP. Coupled-mode theory for optical waveguides: an overview. J Opt Soc Am A 1994; 11 (3): 963–983. doi: 10.1364/JOSAA.11.000963

[23] Rahimi-Keshari S, Broome MA, Fickler R, Fedrizzi A, Ralph TC, et al. Direct characterization of linear-opticalnetworks. Opt Express 2013; 21 (11): 13450–13458. doi: 10.1364/OE.21.013450

[24] O'Brien JL, Pryde GJ, Gilchrist A, James DFV, Langford NK, et al. Quantum Process Tomography of a Controlled-NOT Gate. Phys Rev Lett 2004; 93: 080502. doi: 10.1103/PhysRevLett.93.080502

[25] Guo X, Zou Cl, Schuck C, Jung H, Cheng R, et al. Parametric down-conversion photon-pair source on a nanophotonicchip. Light: Science & Applications 2017; 6 (5): e16249–e16249. doi: 10.1038/lsa.2016.249

[26] Grosso G, Moon H, Lienhard B, Ali S, Efetov DK, et al. Tunable and high-purity room temperature single-photonemission from atomic defects in hexagonal boron nitride. Nat Commun 2017; 8 (1): 1–8. doi: 10.1038/s41467-017-00810-2

[27] Pernice W, Schuck C, Minaeva O, Li M, Goltsman G, et al. High-speed and high-efficiency travelling wave single-photon detectors embedded in nanophotonic circuits. Nat Commun 2012; 3: 1325. doi: 10.1038/ncomms2307

[28] Marsili F, Verma VB, Stern JA, Harrington S, Lita AE, et al. Detecting single infrared photons with 93% system efficiency. Nature Photonics 2013; 7 (3): 210. doi: 10.1038/nphoton.2013.13